Characterization and Calculation of a Cytochrome *c*−Cytochrome b_5 Complex Using NMR Data†

Shashank Deep,‡,§ Sang-Choul Im,§ Erik R. P. Zuiderweg,*,‡ and Lucy Waskell*,§

Department of Anesthesiology, University of Michigan, VA Medical Center, 2215 Fuller Road, Ann Arbor, Michigan 48105, and Biophysics Research Division, University of Michigan, 930 North University Avenue, Ann Arbor, Michigan 48109

Received March 15, 2005; Revised Manuscript Received June 1, 2005

ABSTRACT: To identify the binding site for bovine cytochrome b_5 (cyt b_5) on horse cytochrome *c* (cyt *c*), cross-saturation transfer NMR experiments were performed with ^{2}H- and ^{15}N-enriched cyt *c* and unlabeled cyt b_5. In addition, chemical shift changes of the cyt *c* backbone amide and side chain methyl resonances were monitored as a function of cyt b_5 concentration. The chemical shift changes indicate that the complex is in fast exchange, and are consistent with a 1:1 stoichiometry. A K_a of $(4 \pm 3) \times 10^5$ M^{-1} was obtained with a lower limit of 855 s^{-1} for the dissociation rate of the complex. Mapping of the chemical shift variations and intensity changes upon cross-saturation NMR experiments in the complex reveals a single, contiguous interaction interface on cyt *c*. Using NMR data as constraints, a protein docking program was used to calculate two low-energy model complex clusters. Independent calculations of the effect of the cyt b_5 heme ring current-induced magnetic dipole on cyt *c* were used to discriminate between the different models. The interaction surface of horse cyt *c* in the current experimentally constrained model of the cyt *c*−cyt b_5 complex is similar but not identical to the interface predicted in yeast cyt *c* by Brownian dynamics and docking calculations. The occurrence of different amino acids at the protein−protein interface and the dissimilar assumptions employed in the calculations can largely account for the nonidentical interfaces.

Electron transfer reactions play an essential role in numerous important biological processes such as photosynthesis and respiration and typically involve the transport of electrons through a series of distinct protein−protein complexes. Interaction between cytochrome *c* (cyt *c*)[1] and cytochrome b_5 (cyt b_5) is an excellent model system for studying biological electron transfer reactions. Both reactants are structurally well-characterized and amenable to computer and wet laboratory experiments. The experimental and theoretical investigation of the interaction between these two proteins has provided considerable insight into the manner in which these proteins recognize and bind to each other (reviewed in ref *1*). The strong pH and ionic strength dependence of the cyt *c*−cyt b_5 association (*2*−*4*) suggests that electrostatic interactions play an important part. The crystal structures of cyt *c* and cyt b_5 reveal that the heme groups in both proteins are surrounded by a conserved set of charged amino acid residues. The surface at the predicted interface of cyt *c* has a number of lysine residues that complement the conserved negatively charged regions of cyt b_5. On the basis of modeling studies of the interaction of tuna cyt *c* and bovine cyt b_5, Salemme (*5*, *6*) proposed that four intermolecular complementary electrostatic interactions would result in formation of a 1:1 cyt *c*−cyt b_5 complex with geometry appropriate for electron transfer. In the resulting model, there is displacement of several water molecules from the surface of each protein and the heme prosthetic groups of the molecules are oriented in nearly the same plane with a tilt of approximately 15°. As a result of this model, attention was focused on the experimental characterization [kinetic studies (*2*−*4*, *7*), hyperbaric spectroscopy (*8*−*10*), electrochemistry (*11*), site-directed mutagenesis (*12*−*14*), fluorescence quenching (*15*−*17*), potentiometric titrations (*4*), chemical cross-linking (*1*, *7*, *8*, *18*), and theoretical modeling studies such as molecular and Brownian dynamics (*3*, *13*, *19*, *20*)] of the interaction of these two proteins. Subsequently, many of the features predicted by this model have been demonstrated.

However, the exact extent of the surface area of cyt *c* involved in the recognition of cyt b_5 has never been experimentally determined. Furthermore, the question of which forces are contributing significantly to the stability of complex is still open. It has been suggested by several investigators that complex geometries different from the one described by Salemme can be invoked to explain the experimental results, and that more than one complex configuration might be present in solution (*3*, *13*). The model obtained by Northrup et al. using Brownian dynamics simulation calculations on yeast iso-1-cyt *c* and bovine cyt b_5 (*13*) predicted that the two proteins approach each other with two different docking geometries. One of the complexes incorporated a set of salt bridges similar to those of the Salemme model.

† Supported by a Veterans Administration Merit Review and NIH Grant GM35533 (L.W.) and NIH Grant GM63027 (E.R.P.Z.).

* To whom correspondence should be addressed. Phone: (734) 769-7100, ext. 5858. E-mail: waskell@umich.edu or zuiderwe@umich.edu.

‡ Biophysics Research Division, University of Michigan.

§ Department of Anesthesiology, University of Michigan, VA Medical Center.

[1] Abbreviations: NMR, nuclear magnetic resonance; HSQC, heteronuclear single-quantum coherence; cyt *c*, cytochrome *c*; cyt b_5, soluble domain of cytochrome b_5; EM, energy minimization; AIRs, ambiguous interaction restraints; rmsd, root-mean-square deviation.

10.1021/bi050482x CCC: $30.25
Published on Web 07/16/2005

However, the second complex which was a slightly translated complex compared to the first was significantly more stable and was dominated by an alternate set of salt bridges between the proteins.

There has been only limited success using crystallography to study electron transfer complexes of moderate affinity that are dominated by electrostatic contacts. Even if the structure of a crystalline complex could be obtained, it is likely it would represent only one of a number of productive associations. Therefore, the structural characterization of the cyt *c*−cyt b_5 complex and other electron transfer complexes has been performed largely by NMR spectroscopy (*20*−*24*). Furthermore, the recent publication of sophisticated programs has made it possible to conduct docking simulations using X-ray and NMR data. Mapping the perturbation of chemical shifts upon complex formation provides a highly sensitive tool for identifying the residues that play a role in interprotein interactions. ^{1}H NMR spectroscopy has already provided evidence of an intermolecular interaction, first through hyperfine-shifted signals (*25*) and then through two-dimensional ^{1}H NMR spectroscopy (*26*, *27*). Later, as ^{15}N-enriched cyt b_5 and cyt *c* became available, HSQC experiments were performed in the presence of each other to monitor changes in the backbone chemical shift upon complexation (*20*, *28*). Recently, NMR studies have been carried out on ^{15}N- and ^{13}C-enriched cyt b_5 which was titrated with unlabeled cyt *c* to monitor chemical shift changes in not only the backbone but also the side chain methyl groups. Cross-saturation transfer experiments, which delineated only a single binding site on cyt b_5 for cyt *c*, have also been conducted (*29*).

In the work presented here, the NMR studies have been extended by monitoring a full titration series of ^{15}N- and ^{13}C-enriched ferrous cyt *c* with the unlabeled ferrous cyt b_5 to identify residues on horse cyt *c* which interact with bovine cyt b_5. From these data, the association constant and the lower limit of k_{off} were calculated. The chemical shift changes induced in cyt *c* upon titration with cyt b_5 were mapped onto the structure to identify the residues affected by complex formation. A recently developed computer program, HADDOCK (*30*), allowed us to use the NMR data to provide a model of the interaction surface. Our docking predicts the formation of salt bridges between Lys72 of cyt *c* and Asp60 of cyt b_5, Lys73 of cyt *c* and Glu56 and Asp60 of cyt b_5, Lys86 of cyt *c* and Glu43 and Glu44 of cyt b_5, Lys87 of cyt *c* and Glu48 of cyt b_5, and Lys88 of cyt *c* and Glu44 of cyt b_5.

Docking in which surface residues are allowed to move coupled to NMR mapping is now a well-established method for studying protein−ligand interactions and is a promising approach for drug design. Heteronuclear NMR and docking calculations have been used by other investigators to build structural models of complexes of electron transfer proteins, for example, cytochrome c_{553}−ferredoxin (*31*), cytochrome c_{533}−[Fe] hydrogenase (*32*), cytochrome b_5−myoglobin (*23*), and cytochrome *c*−cytochrome *f* (*33*).

EXPERIMENTAL PROCEDURES

Materials. Yeast extract and tryptone for *Escherichia coli* growth media were obtained from Fisher Scientific. Restriction endonucleases were from New England Biolabs (Beverly, MA). T4 DNA ligase and ligase buffer were from Stratagene. The Qiagen minikit was used for DNA extraction. Chloramphenicol, glycerol, and potassium phosphate were from Fisher Scientific. Carbenicillin, isopropyl β-D-thiogalactopyranoside, and δ-aminolevulinic acid were from RPI (Mount Prospect, IL). All chemicals used for medium supplements and for the vitamin mix were purchased from Sigma. Sepharose CL-6B and G-75 resins were from Sigma. Deuterium oxide, isotope-labeled Martek-9 media (^{15}N, ^{13}C and ^{15}N, or ^{2}H and ^{15}N), [^{13}C]glycerol, and [^{15}N]ammonium sulfate were from Spectra Stable Isotopes (Columbia, MD). Plasmids pBTR horse cyt *c*, pBTR(horse cyt *c*), and pEC86 were kindly supplied by G. J. Pielak (University of North Carolina, Chapel Hill, NC) and L. Thöny-Meyer (Institute of Microbiology, Zurich, Switzerland), respectively.

Expression of ^{15}N-Enriched and ^{13}C-, ^{15}N-Enriched Horse Cyt c. Unless otherwise specified, all DNA manipulations were performed as described previously (*34*). Horse cyt *c* was overexpressed in *E. coli* C41 cells (*35*) using the pLW01 plasmid containing the horse cyt *c* and yeast, *Saccharomyces cerevisiae*, heme lyase gene (*36*). The pLW01-cyt *c*-heme lyase plasmid was constructed by excising the horse 1-cyt *c* and heme lyase genes from pBTR (horse cyt *c*) (a generous gift from G. J. Pielak) (*37*) and cloning it into the *Nco*I and *Hin*III restriction sites of pLW01 (*36*). The sequence of the cyt *c* and heme lyase gene was confirmed by double-stranded sequencing of the genes. The pLW01-cyt *c*-heme lyase plasmid was transformed into C41 cells. Following overnight incubation at 37 °C, a single colony was picked from a Luria Broth (LB) plate containing carbenicillin at a final concentration of 0.24 mM. The single colony was inoculated into 10 mL of Terrific Broth (TB) containing 0.24 mM carbenicillin and incubated for 16 h at 37 °C with shaking at 250 rpm. The cells were pelleted and gently resuspended in 10 mL of fresh Martek-9N or -9CN medium for ^{15}N-enriched and ^{13}C- and ^{15}N-enriched media, respectively. One milliliter of the resuspended cells was subsequently transferred into 100 mL of Martek-9N or -9CN medium. The Martek-9N and -9CN media contained 90 mL of the appropriate Martek solution, 9 mL of 1 M potassium phosphate buffer (pH 7.2), 0.8 mL of 50% glycerol ([^{13}C]glycerol was used for ^{13}C enrichment), 0.24 mM carbenicillin, 0.2 g of $(NH_4)_2SO_4$ ([^{15}N]ammonium sulfate used when ^{15}N was required), 1 mM $CaCl_2 \cdot 7H_2O$, 10 mM $MgSO_4$, 10 μM $FeCl_3 \cdot 6H_2O$, 25 μM $ZnSO_4 \cdot 7H_2O$, 20 μM $MnCl_2 \cdot 4H_2O$, 500 μM δ-aminolevulinic acid, and vitamin mix (25 μg of biotin, choline chloride, folic acid, niacinamide, pyridoxal·HCl, riboflavin, and D-pantothenic acid and 500 μg of thiamine).

Optimal expression was achieved with a 100 mL culture volume in a 500 mL Erlenmeyer flask. The flasks containing 100 mL of the expression medium were incubated at 35 °C with shaking at 250 rpm until the OD at 600 nm was 1.5−1.8. Isopropyl β-D-thiogalactopyranoside was added to a final concentration of 250 μM, and the incubation was continued for 16 h at which time the cells were harvested.

Expression of [^{2}H,^{15}N]Horse Cyt c with and without δ-Aminolevulinic Acid. The pLW01-horse cyt *c*-heme lyase plasmid and C41 cells were used for expression in the presence of δ-aminolevulinic acid as described above except for the following modifications. *E. coli* C41 cells will not grow in 100% deuterated medium unless they have been "trained" to grow on increasing deuterium oxide concentra-

tions. Transformed C41 cells were successively grown on LB, 0.24 mM carbenicillin plates containing 10, 20, 30, and 50% deuterium oxide. A single colony from a plate made with 50% deuterium oxide was transferred into 10 mL of 100% deuterated TB medium containing 0.24 mM carbenicillin. The culture was incubated at 37 °C with shaking at 250 rpm for 20 h. Growth is slower in medium containing 100% deuterium oxide. The cells were pelleted and resuspended in 10 mL of fresh Martek-9DN medium containing the same ingredients (minerals, vitamins, etc.) described for expressing [^{15}N]- and [^{13}C,^{15}N]cyt *c*. One milliliter of the resuspended cells was transferred to 100 mL of Martek-9DN medium and incubated at 35 °C with shaking at 250 rpm until the absorbance at 600 nm was 1.5−1.8 (≅25 h). Isopropyl β-D-thiogalactopyranoside was added to a final concentration of 100 μM, and the incubation was continued for 37 h at 30 °C with shaking at 200 rpm. The NMR saturation transfer experiments revealed that cyt *c* purified from these cells contained heme that was not completely deuterated. The heme contained a significant number of protons. Presumably, the unlabeled heme precursor δ-aminolevulinic acid was incorporated directly into the heme.

To express cyt *c* containing deuterated heme, the pLW01-horse cyt *c*-heme lyase plasmid was coexpressed with the pEC86 plasmid which contains the eight genes required for cyt *c* heme maturation (*ccm*ABCDEFGH) (*38*). The plasmid was a generous gift from Dr. L. Thöny-Meyer. Coexpression of the pEC86 and pLW01-horse cyt *c*-heme lyase plasmids in C41 cells enabled us to express cyt *c* in good yields in the absence of unlabeled δ-aminolevulinic acid, thereby increasing the level of deuteration of the heme. *E. coli* C41 cells containing both plasmids were selected on LB plates containing carbenicillin (0.24 mM) and chloramphenicol (50 μg/mL) and grown as described in the previous paragraph with the addition of chloramphenicol and elimination of δ-aminolevulinic acid from the growth medium.

Purification of Cyt c. The C41 cells from 1 L of culture were harvested at the appropriate times. They were pelleted at 30000*g* and 4 °C for 15 min. The purification was conducted at 4 °C. The supernatant was discarded, and the cells were resuspended in 60 mL of B-per (Pierce) with 3 protease inhibitor cocktail tablets (Roche) and 30 mg of lysozyme. The solution was incubated on ice for 1 h and then held at −20 °C. Subsequently, the cells were defrosted and then lysed by sonication. Cell debris was removed by centrifugation at 24000*g* for 30 min. The supernatant was removed and saved. The pellet was resuspended in 40 mL of 46 mM potassium phosphate buffer (pH 7.0) at 4 °C (buffer A). The sonication and resuspension procedure was repeated approximately four times until more than 95% of the cyt *c* had been extracted from the original cell pellet. A CM-Sepharose CL-6B column (3 cm × 15 cm) was pre-equilibrated with 200 mL of buffer A. The combined supernatants from the sonicated cells were pooled and diluted with water until the conductivity was equal to that of buffer A. The cyt *c* was loaded onto the column at ≅1 mL/min. The column was washed with buffer A until a yellow compound eluted (≅400 mL of buffer A). Cyt *c* was then eluted with a solution of buffer A and 0.5 M NaCl. The red fractions were pooled and concentrated to <10 mL in an Amicon concentrator fitted with a YM5 membrane. The protein was loaded onto a G-75 column (3 cm × 90 cm) pre-equilibrated with 1 L of 20 mM potassium phosphate buffer (pH 7) at 4 °C (buffer B). The cyt *c* was eluted with buffer B. The fractions containing >1 μM cyt *c* were pooled and concentrated to <5 mL. An extinction coefficient of 106.1 mM^{-1} cm^{-1} at 410 nm was used to quantitate cyt *c* (*39*). A few grains of potassium ferricyanide (Sigma) were added to oxidize the protein. The cyt *c* was further purified by HPLC (Waters 650E) on a cationic S-10153 column (Bio-Rad) using a gradient from 100% buffer A to 100% buffer D [10 mM potassium phosphate buffer (pH 7) containing 1 M NaCl] over the course of 55 min. The 280 nm peak at 25% buffer D and 75% buffer A was collected. The buffer in which cyt *c* eluted was exchanged to a 1 mM potassium phosphate (pH 7) solution. Two micrograms of the cyt *c* ran as a single band on a 15% SDS−polyacrylamide gel. The protein was concentrated to 3 mM on an Amicon concentrator, filtered through a 0.22 μm sterile filter, and stored at −20 °C. A Bio-Rad protein assay kit was used to measure the total protein concentration.

From 1 L of cell culture, it was possible to isolate 24, 26, and 14 mg of pure [^{15}N]-, [^{13}C,^{15}N]-, and [^{2}H,^{15}N]cyt *c*, respectively, with an overall yield from the cell culture averaging ≅25%. The molecular mass of the enriched proteins was determined by MALDI-TOF (matrix-assisted laser desorption ionization time-of-flight) mass spectrometry.

The molecular masses were 12 448 ± 12, 12 638 ± 12, and 13 053 ± 13 Da for [^{15}N]cyt *c* (99% enriched), [^{13}C,^{15}N]cyt *c* (96% enriched), and [^{2}H,^{15}N]cyt *c* (99% enriched when grown with δ-aminolevulinic acid), respectively. Interestingly, the ^{2}H- and ^{15}N-enriched sample prepared in the absence of δ-aminolevulinic acid had a molecular mass of 12 166 ± 12 Da, indicating it was only 97% labeled.

Preparation of Ferrous Cyt c Samples for NMR. The reduced NMR samples were prepared under anaerobic conditions in a glovebox. The required amount of isotope-enriched cyt *c* and unlabeled cyt b_5 in 1 mM potassium phosphate buffer (pH 7.0) were aliquoted into a microcentrifuge tube from a concentrated solution. A solution of sodium dithionite, the concentration of which was known, was used to stoichiometrically reduce the cyt b_5 and cyt *c*. When the proteins were reduced, a 1.1−1.5-fold molar excess of dithionite was added. Depending on the sample, the pH was then adjusted with KOH, KOD, HCl, or DCl to pH 7 on the pH meter. Potassium phosphate buffer (1 mM) in the appropriate solvent, D_2O or H_2O, was added to 700 μL. The sample was transferred to a Wilmad NMR tube in the glovebox and capped with a rubber stopper. Outside the glovebox, the glass NMR tube was sealed under a positive pressure of nitrogen with a propane−oxygen torch.

NMR Experiments. The NMR experiments were carried out at 25 °C on a Bruker Avance 600 spectrometer equipped with a triple-resonance gradient probe unless stated otherwise.

^{1}H−^{15}N fast-WATERGATE-HSQC spectra of ^{15}N- and ^{13}C-enriched ferrous cyt *c* unbound and in complex with cyt b_5 in 1 mM potassium phosphate buffer (pH 7) at different cyt *c*:cyt b_5 ratios were recorded with a spectral width of 7692 Hz for ^{1}H and 1773 Hz for ^{15}N as an array of 4K × 200 complex points. ^{1}H−^{13}C CT-HSQC spectra for ^{13}C- and ^{15}N-enriched ferrous cyt *c* alone and in complex with unlabeled cyt b_5 were collected with a spectral width of

8333.3 Hz and 4K complex points in the ^{1}H dimension, and with a spectral width of 10 000 Hz and 480 complex points in the ^{13}C dimension.

A three-dimensional (3D) HNCA spectrum of ^{15}N- and ^{13}C-enriched ferrous cyt *c* was recorded with spectral widths of 7505, 1785, and 7505 Hz for ^{1}H, ^{15}N, and ^{13}C, respectively, on a Bruker Avance 500 spectrometer. A 3D CCCCONH spectrum was recorded with spectral widths of 9615, 1825, and 10562 Hz for ^{1}H, ^{15}N, and ^{13}C, respectively. A 3D HCCCCONH spectrum was recorded with spectral widths of 9615, 1825, and 4200 Hz for ^{1}H, ^{15}N, and aliphatic protons, respectively.

The NMR spectra were processed using NMRPipe (*40*) and analyzed with SPARKY (*59*). In general, the time domain data were zero-filled in the indirect dimensions and apodized with shifted sine bell or Lorentzian-to-Gaussian window functions. Linear prediction was applied to indirect heteronuclear dimensions acquired with constant-time evolution. Molecular representations were made with MOLMOL (*41*).

Analysis of Chemical Shift Changes. Chemical shifts of cyt *c* in the complex with cyt b_5 were compared with the confirmed resonance assignments of cyt *c* alone. All NMR experiments were conducted in 1 mM potassium phosphate buffer (pH 7). The binding constant, K_a for cyt *c* and cyt b_5, was determined from the data using eq 1:

$$\Delta\delta = \Delta\delta_\infty(-B - \sqrt{B^2 - 4ab})/(2a) \quad (1)$$

where

$$B = -(a + b + 1/K_a) \quad (2)$$

and *a* and *b* are the total concentrations of cyt *c* and cyt b_5, respectively, $\Delta\delta$ is the chemical shift change of a cyt *c* residue upon addition of cyt b_5, and $\Delta\delta_\infty$ is the estimated chemical shift change for the state where $b/a \rightarrow \infty$. K_a is the equilibrium association constant assuming a bimolecular interaction.

Composite chemical shift differences for cyt *c* amide ^{1}H and ^{15}N chemical shifts upon cyt b_5 binding were calculated using the equation $\Delta\delta(\mathrm{NH}) = \{[\Delta\delta\mathrm{H}^2 + (\Delta\delta\mathrm{N}/5)^2]/2\}^{1/2}$, where $\Delta\delta$H and $\Delta\delta$N are the differences in chemical shift observed between the bound and free states. The corresponding weighted averages for the side chain methyl groups were calculated using the equation $\Delta\delta(\mathrm{CH}) = \{[\Delta\delta\mathrm{H}^2 + (\Delta\delta\mathrm{C}/4)^2]/2\}^{1/2}$, where $\Delta\delta$H and $\Delta\delta$C are the chemical shift differences observed for the methyl protons and carbons, between the bound and free states. The composite shift differences were mapped onto the structure of cyt *c*.

The cross-saturation NMR experiments were performed on samples containing 0.8 mM ferrous [^{2}H,^{15}N]cyt *c* in 1 mM potassium phosphate (pH 7.0) in a 1:1 H_2O:D_2O mixture alone or with 0.96 mM cyt b_5 on a Varian Inova spectrometer at 18.1 T (800 MHz ^{1}H) as described by Shimada and coworkers (*42*). To maximize the magnetization transfer, the temperature was reduced to 15 °C. The saturation of aliphatic protons of cyt b_5 was achieved with a 2.4 s train of iburp-2 pulses of 6 ms separated by 6 ms delays. Control experiments were carried out to ascertain that the H_2O resonance was not affected by the saturation field. Off-resonance experiments were collected with the center of the decoupling field shifted 20 000 Hz upfield. A high amide proton occupation on the target protein (cyt *c*) was used to obtain a sufficient signal:noise ratio. We have not observed any indications of amide proton−amide proton spin diffusion on the target protein, which would have shown up as an extensive surface patch, and/or as saturation transfer to internal amide protons. Apparently, our choice of solvent conditions and experimental parameters struck the right compromise between sensitivity and selectivity for this particular complex.

Calculation of a Cyt c−Cyt b_5 Complex Using NMR Data. The HADDOCK docking software (*30*) was used to compute the lowest-energy cyt *c*−cyt b_5 complexes using chemical shift mapping and cross-saturation transfer data. HADDOCK CNS scripts were modified to accommodate the heme prosthetic group of cyt *c* and cyt b_5. The topology and parameter files for heme were generated using XPLO2D (*43*−*45*). The charge on the individual heme atoms was assigned using values from the toph19x.heme force field of XPLOR. All force constants in the parameter file were matched to parallhdg.pro of X-PLOR, i.e., 1000 kcal mol^{-1} Å^{-2} for bonds and 500 kcal mol^{-1} Å^{-2} for angles, dihedrals, and impropers. The chemical shift perturbation and cross-saturation data identifying the contact residues of cyt *c* in this work, along with data identifying the contact residues on cyt b_5 (*29*), as derived from the Boolean cross section of chemical shift perturbation, saturation transfer mapping, and change in relaxation parameters for cyt b_5 resonances, were used as input for the docking process with HADDOCK. The docking protocol consisted of three sequential steps. Initially, the cyt *c* (PDB entry 2GIW) and cyt b_5 (PDB entry 1CYO) were positioned 150 Å apart from each other in space. Rigid body energy minimization (EM) was then performed. First, four cycles of orientational optimization were performed in which each protein in turn is allowed to rotate to minimize an artificial intermolecular energy function (see below). Subsequently, both translations and rotations are allowed, and the two proteins were docked by rigid body energy minimization. The intermolecular energy is the sum of electrostatic, van der Waals, and ambiguous intermolecular distance restraint (AIR) energy terms between contact residues on each molecule. Five hundred rigid body docking complex conformations are calculated at this stage. The best 50 solutions in terms of intermolecular energies were then refined. The second stage consists of three simulated annealing refinements in torsion angle space for each of the best 50 structures. In the first simulated annealing (1000 steps from 2000 to 50 K with 8 fs time steps), the two proteins are considered rigid bodies and their respective orientation is optimized. In the second annealing (4000 steps from 2000 to 50 K with 4 fs time steps), side chains at the interface are allowed to move. In the third simulated annealing (1000 steps from 500 to 50 K with 2 fs time steps), both side chains and the backbone at the interface are allowed to move to allow for some conformational rearrangements. The same 50 structures are then subjected to 200 steps of steepest descent energy minimization. The final stage consists of a gentle refinement in Cartesian space with explicit solvent. The final ensemble of 50 structures is analyzed in this paper.

Calculation of the Chemical Shifts Expected from the Docked Structure and the Effect of the Heme Ring Current on the Chemical Shifts of Its Partner. A low-energy model structure of the cyt *c*−cyt b_5 complex was analyzed with

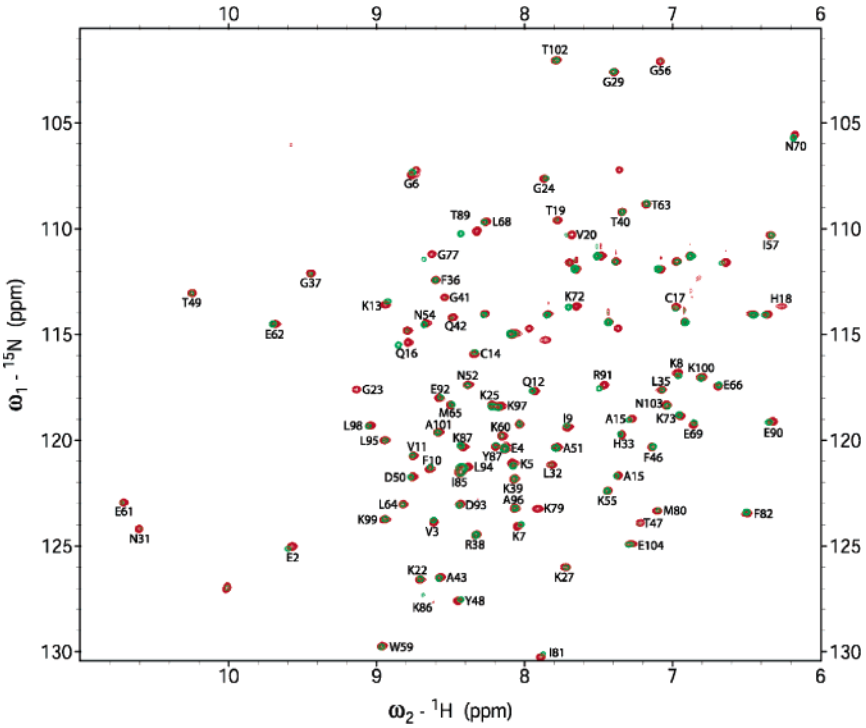

FIGURE 1: Superposition of the amide region of the $^{1}H-^{15}N$ HSQC spectra of 0.8 mM ^{15}N- and ^{13}C-enriched ferrous cyt *c* alone (red) and in the presence of unlabeled ferrous cyt b_5 (green) with a cyt *c*:cyt b_5 ratio of 1:1.2. The cross-peaks are labeled with sequence specific assignments.

ShiftCalc (*46*−*48*) to determine how well the calculated chemical shifts from the model complex agree with the chemical shifts observed experimentally. We computed the amide proton chemical shifts for the NMR structure of reduced horse cyt *c* (2GIW), the crystal structure of bovine cyt b_5 (1CYO), and a model structure obtained from the docking program.

ShiftCalc was also used to evaluate the contributions of the magnetic dipole of the ring current of the heme of cyt b_5 to the chemical shifts observed in cyt *c* by comparing the chemical shifts predicted in the presence of holo cyt b_5 and apo cyt b_5 (cyt b_5 lacking the heme). A similar calculation was conducted to examine the effect of the ring current of the heme of cyt *c* on the chemical shifts of cyt b_5.

RESULTS AND DISCUSSION

Confirmation of the Resonance Assignments for Horse Cyt c. Assignments of backbone resonances and side chain resonances have been reported previously for the H26N/H33N double mutant of horse cytochrome *c* (*49*). Our results for the wild-type protein used in this study are similar to those previously reported except for a few resonances, mostly around the mutated region. The sequential backbone resonance assignments of those residues were obtained and others confirmed using a single 3D HNCA experiment. Side chain assignments were confirmed from the analysis of 3D CCCCONH, HCCCCONH, and HCCH-TOCSY spectra.

Titration of ^{15}N-and ^{13}C-Enriched Cyt c with Unlabeled Cyt b_5. Two-dimensional $^{1}H-^{15}N$ HSQC and $^{1}H-^{13}C$ HSQC spectra were used to monitor the titration of 0.8 mM ^{15}N- and ^{13}C-enriched cyt *c* with unlabeled cyt b_5. A single resonance is observed for each observable amide of cyt *c* at any point during the titration, indicating that the cyt *c*−cyt b_5 complex is in fast exchange on the NMR time scale between its unbound and bound forms. A superposition of the HSQC spectrum of free cyt *c* (red) and complexed with cyt b_5 (cyt *c*:cyt b_5 ratio of 1:1.2, green) is shown in Figure 1. Chemical shift perturbations and increases in line width were observed in the spectrum of cyt *c* upon formation of the complex with cyt b_5. The line width of the $^{1}H-^{15}N$ cross-peaks increased over the range of the titration in a saturable manner, providing strong evidence for a stable intermolecular interaction. However, the increase in the change in chemical shift was followed by a decrease for all resonances upon further addition of cyt b_5. This behavior was attributed to an increase in the ionic strength of the solution which occurs upon addition of cyt b_5. The higher ionic strength weakens the electrostatic interactions between the two proteins and causes partial dissociation of the complex. This is consistent with earlier reports that have demonstrated that complex formation is acutely sensitive to ionic strength and pH (*1*). To decrease the contribution to the ionic strength from the protein source, the titration was repeated using a lower concentration of cyt *c* (0.1 mM) with the cyt *c*:cyt b_5 molar ratio varying from 1:0 to 1:15. An overlay of the HSQC spectra of 0.1 mM cyt *c* with and without cyt b_5 shows the perturbation of the same set of residues observed earlier. However, in this case, the change in chemical shift increased in a saturable manner (Figure 2A).

The changes in the amide proton chemical shifts of cyt *c* with increasing concentrations of cyt b_5 are shown in Figure 2A. The profile of chemical shift variations and intensity change as a function of cyt b_5 matches well what was expected on the basis of the formation of a 1:1 adduct. In contrast to our current results with horse heart cyt *c* and bovine cyt b_5, the profile of chemical shift change on addition of yeast iso-1-cyt *c* to rabbit cyt b_5 by others suggested the possibility of formation of a complex of 2 mol of iso-1-cyt

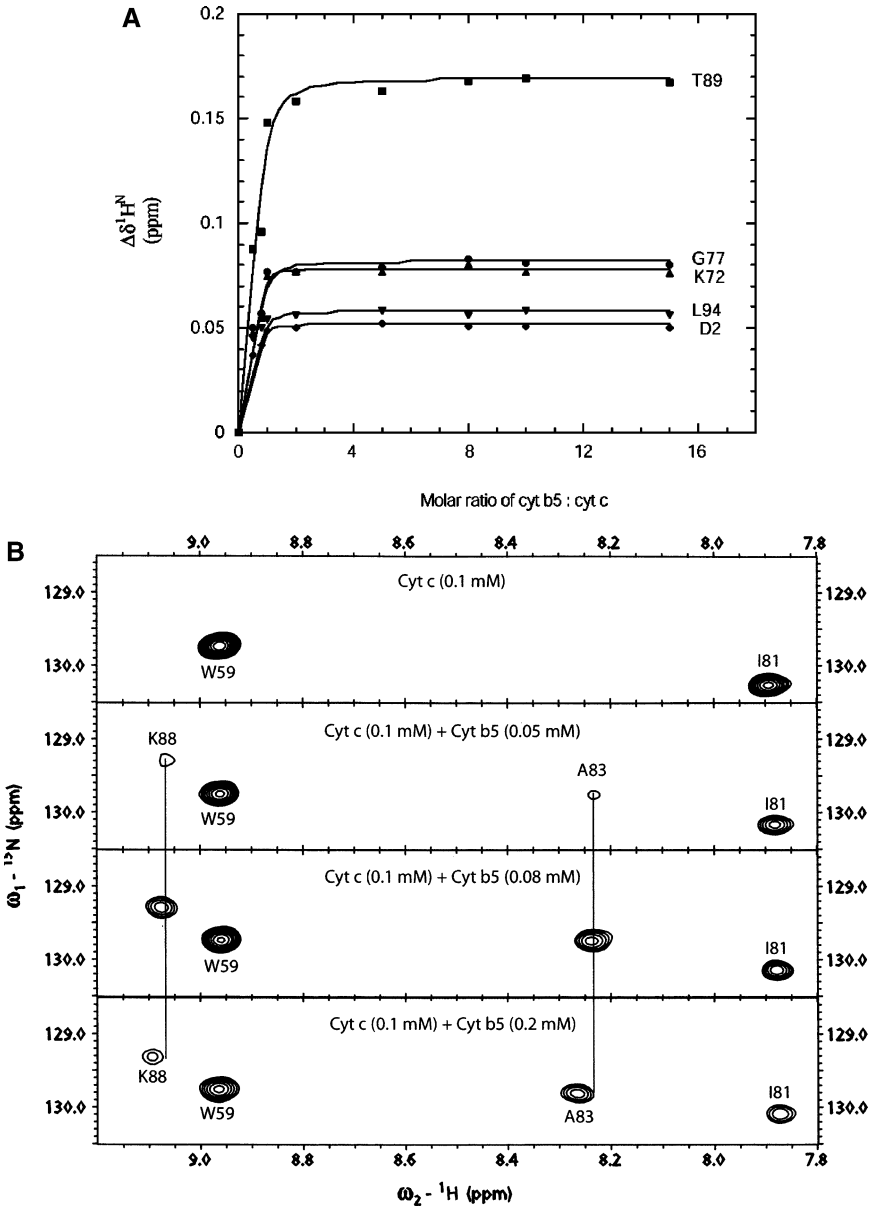

FIGURE 2: (A) Titration curves showing changes in chemical shift for a select number of amide protons of ^{15}N- and ^{13}C-enriched cyt c (0.1 mM) upon addition of unlabeled cyt b_5. The curves represent the best fit of the individual data using eq 1 of the text. (B) A region of the ^{1}H−^{15}N HSQC spectra of ^{15}N- and ^{13}C-enriched ferrous cyt c showing the appearance and shifting of A83 and K88 upon addition of cyt b_5.

c with 1 mol of cyt b_5 at high cyt c:cyt b_5 ratios (*52*). Thus, the experimental result may vary depending on the source of the cyt b_5 and cyt c proteins.

Analysis of the chemical shift changes indicates an equilibrium association constant of $(4 \pm 3) \times 10^5$ M^{-1} with a 1:1 stoichiometry. The uncertainty represents the variability of fitting amide proton chemical shift changes for five different residues.

A range of affinity constants for the cyt c−cyt b_5 complex can be found in the literature, depending upon the source of the proteins involved in the complexes and the differences in conditions under which the measurements are taken. The value of K_a obtained in this study is 1 order of magnitude larger than the one we reported when labeled cyt b_5 (0.8 mM) was titrated with unlabeled cyt c (*29*). The difference between the observed binding constants can be attributed to the overall lower ionic strength of the solution when ^{15}N- and ^{13}C-enriched cyt c (0.1 mM) is titrated with cyt b_5. The interaction between the two cytochromes is strongly dependent on ionic strength. However, assessing the ionic strength for solutions containing the high concentrations of charged proteins required for these experiments in the presence of low salt concentrations is not reliable.

Two amide resonances (Ala83 and Lys88), which were absent in the spectrum of free cyt c, appeared when unlabeled cyt b_5 was added to the solution (Figure 2B). Comparison of two spectra with different concentrations of cyt b_5 indicates that Ala83 and Lys88 undergo chemical shift changes with the addition of cyt b_5. It thus appears that millisecond conformational fluctuations of these residues in free cyt c were perturbed by binding to cyt b_5. Milli- to microsecond motions have often been observed by NMR spectroscopy at protein surfaces that are destined to be interfaces in complexes (*50*).

The maximum chemical shift change, 136 Hz, occurring in the complex was observed for the amide proton of Thr89.

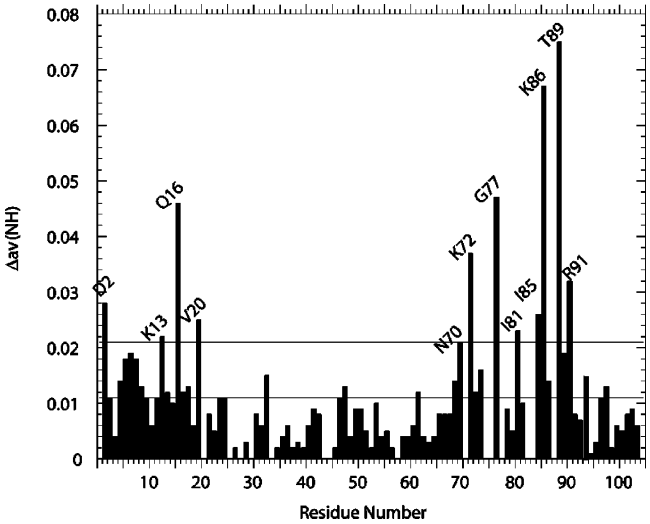

FIGURE 3: Composite chemical shift difference, as defined by eq 1, of the ^{15}N and ^{1}H backbone amide resonances of cyt *c* upon complexation with cyt b_5. The bottom line represents the mean chemical shift change, and the top line at 0.021 ppm represents the mean value plus one standard deviation. Residues with composite chemical shift changes of >0.021 ppm are considered significantly affected upon complex formation and are color-coded in Figure 4.

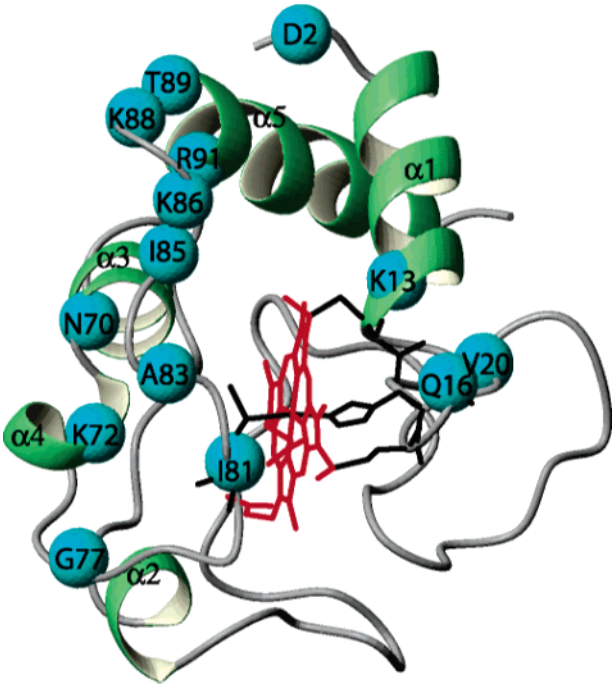

FIGURE 4: Ribbon representation of the solution structure of horse heart ferrous cyt *c* (PDB entry 2GIW). The residues that exhibited a composite chemical shift difference of the amide group greater than the mean value plus one standard deviation and Lys88 and Ala83 which appeared and then shifted (see Figure 3) are mapped as blue spheres and labeled. The heme is colored red, and the bonds connecting the heme to the axial ligands and covalent bond with two cysteines are colored black. This figure was prepared with MolMol (*41*).

This suggests a lower limit for the dissociation rate (k_{off}) of 855 s^{-1} ($k_{off} \gg 2\pi\Delta\delta$, where $\Delta\delta$ is the maximum observed difference in chemical shift between the free and complexed form of cyt *c*).

Chemical Shift Changes Observed on Cyt c upon Complex Formation. The chemical shift changes induced in cyt *c* by cyt b_5 binding were mapped using the composite chemical shift differences of the backbone amide ^{1}H and ^{15}N resonances and are shown in Figure 3. The chemical shift perturbations of the amide protons are large relative to the chemical shifts of the amide protons observed for cyt b_5 (*29*). In a later section, we demonstrate this is likely due to the larger effect of the ring current of the solvent-exposed heme of cyt b_5 on the resonances of cyt *c* as compared to the smaller effects of the largely buried heme of cyt *c* on the resonances of cyt b_5.

As shown in Figure 4, the structure of cyt *c* is characterized by five α-helices (residues 3−13, 50−53, 63−69, 71−74, and 89−101) connected by loops. The two axial iron ligands belong to the first and last loops. The largest composite chemical shifts are observed for Asp2 and Lys13 in helix α1, Gln16 and Val20 in the loop connecting helices α1 and α2, Asn70 in the loop connecting helices α3 and α4, Lys72 in α4, Gly77, Ile81, Ile85, Lys86, and Thr89 in the loop connecting helices α3 and α4, and Arg91 in helix α5. As side chains commonly play a dominant role in molecular recognition, we have investigated the chemical shift changes for the side chain methyl protons of cyt *c* upon complexation with cyt b_5. The ^{1}H−^{13}C HSQC spectrum of cyt *c* overlaid on that of the cyt *c*−cyt b_5 complex is depicted in Figure 1B in the Supporting Information. There are only a few side chain resonances which become perturbed upon addition of cyt b_5. These include side chains I81γ, I81δ, A83β, I85γ, and I85δ; all of them are located in the loop between helices α4 and α5.

The competitive paramagnetic difference spectroscopy experiments carried out by others (*25*), in which $[Cr(oxalate)_3]^{3-}$ and $[Cr(CN)_6]^{3-}$ were used as competitors for cyt b_5, have been useful in delineating the interacting region of cyt *c* for cyt b_5. At pH 7.2, the main interaction surface on cyt *c* for cyt b_5 was shown to include Lys72, Ile81, Ala83, Phe82, and Ile85, which is consistent with our results. Comparison of the crystal structures of oxidized and reduced forms of horse heart cyt *c* reveals that Gln16, Lys87, and Glu90 undergo significant conformational changes with a change in oxidation state. These residues have also been shown to be in contact with residues of cytochrome *c* peroxidase in the crystal structure of the cyt *c*−cyt *c* peroxidase complex (*51*).

Residues showing perturbations in the HSQC spectra are located near the solvent-exposed heme and form a large single patch on the surface of cyt *c*. Among them, are two of the three pairs of conserved positively charged lysines surrounding the solvent-exposed heme, with no significant chemical shift changes for the other pair of conserved lysines, Lys27 and Lys79, and nearby residues.

Panels A−D of Figure 5 show the residues on cyt *c* implicated in binding cyt b_5 in this work and from the models and experiments in the literature. The backbones of the three forms of cyt *c* were superimposed; all molecules are shown with the heme in the same orientation, and residues are numbered as in horse cyt *c*. The interface region identified here for horse cyt *c* is different from that proposed by Salemme for tuna cyt *c* (*5*), and instead close to the alternative, more stable, structure predicted by Brownian dynamics simulations of Northrup using yeast iso-1-cyt *c* (*13*). It is to be noted that the interprotein interfaces of cyt b_5 in the Northrup and Salemme model are very similar. A

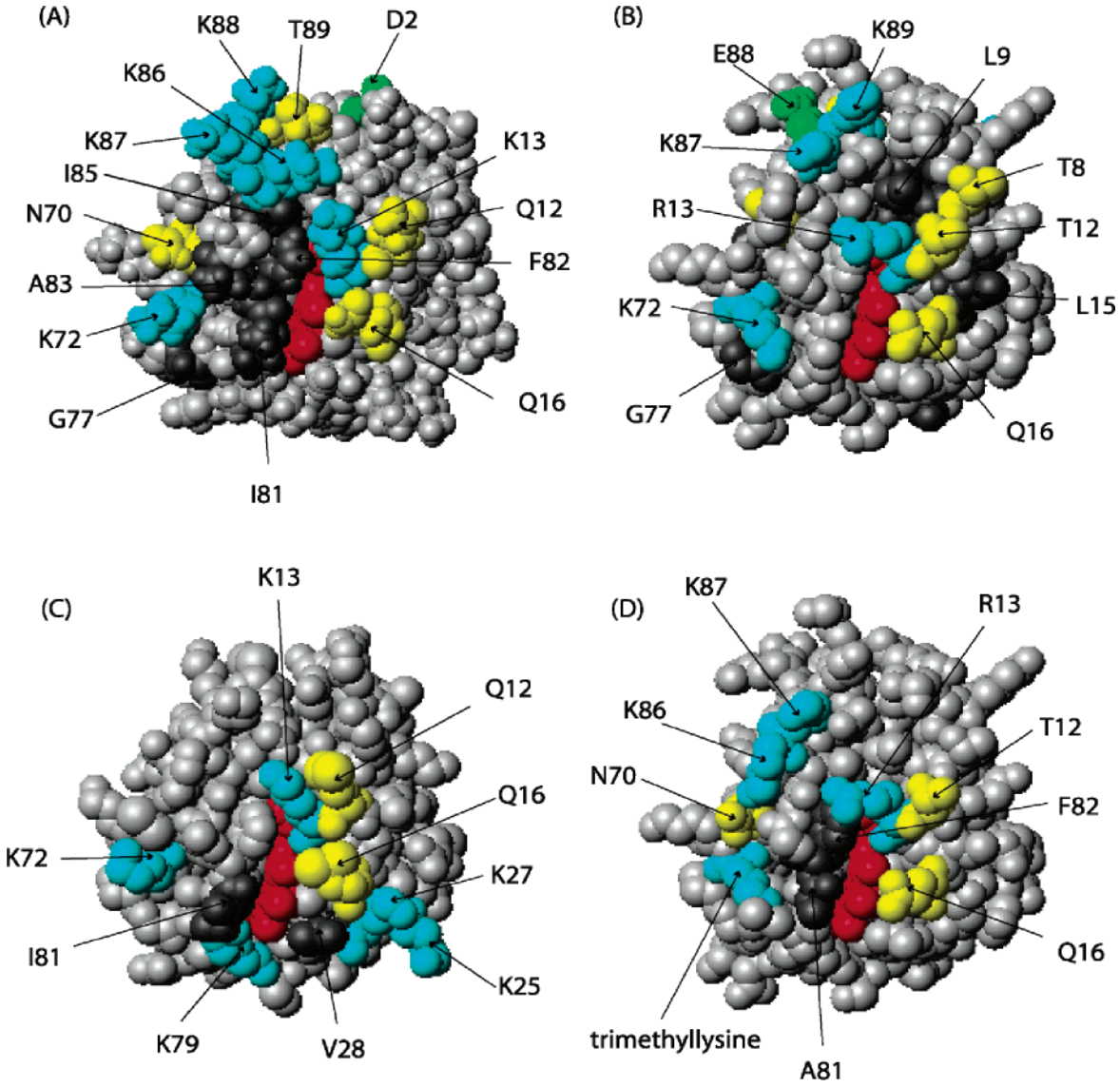

FIGURE 5: Display of the surfaces of different species of cyt *c* showing interfacial residues predicted from (A) cross-saturation transfer and chemical shift mapping results in this work with horse cyt *c*, (B) chemical shift mapping results from an earlier study by others on yeast iso-1-cyt *c* (*52*), (C) the Salemme model on tuna cyt *c* (*5*), and (D) the Northrup model on yeast trimethyllysine iso-1-cyt *c* (*13*). Positive, negative, polar, and apolar interfacial residues are colored cyan, green, yellow, and dark gray, respectively. This figure was prepared with MolMol (*41*).

chemical shift mapping study is also available on the interaction between ^{15}N-enriched reduced yeast iso-1-cyt *c* and ferrous rabbit cyt b_5 (*52*). The interprotein interface is close to, but different from, those experiencing the largest shifts in this work, presumably indicating a slightly different interface. In the studies described above, rabbit cyt b_5 induces a large number of chemical shift changes which are primarily near the heme but also on the backside of yeast cyt *c* away from the heme. Nevertheless, the perturbed residues near the heme are the same in both the Banci and Northrup model.

Cross-Saturation Transfer NMR Experiments with the Cyt c−Cyt b_5 Complex. The cross-saturation transfer experiment (*42*, *53*) is a way to reliably and directly identify residues in contact at the protein−protein interface. It provides more direct evidence of an interprotein interface than chemical shift mapping which may identify buried residues indirectly affected by binding. The cross-saturation experiment utilizes an isotope labeling scheme in which a protein (cyt *c*), whose interface residues are to be identified, is uniformly enriched with ^{2}H and ^{15}N. The enriched protein is complexed with a nonlabeled target protein (cyt b_5) in a solvent containing a mixture of H_2O and D_2O. The partially protonated solvent will replace some of the exchangeable amide deuterons of cyt *c* with protons so that the correlation between the amide nitrogen and amide proton can be observed. In an attempt to obtain [^{2}H,^{15}N]cyt *c* with a perdeuterated heme, a cyt *c*-containing plasmid was coexpressed with a plasmid encoding all of the cyt *c* maturation genes. This enabled the cyt *c* to be expressed at significant levels in the absence of unlabeled δ-aminolevulinic acid (*38*). The NMR experiment consists of a steady-state saturation of the aliphatic proton resonance spectral region followed by a ^{1}H−^{15}N HSQC experiment (on-resonance experiment). Since the cyt *c* aliphatic and heme protons are replaced with deuterons, this irradiation results in selective saturation of the aliphatic protons of the nonlabeled cyt b_5. Intramolecular cross-relaxation carries the saturation from the aliphatic protons of cyt b_5 to other protons of cyt b_5. Amide protons on cyt *c*

that are in the proximity of saturated cyt b_5 protons will become partially saturated through intermolecular cross-relaxation over the interface of the complex. The intensity of the amide peaks (I_{on}) in the experiment in which the aliphatic hydrogens are saturated (on-resonance experiment) was compared with the intensity of the amide peaks (I_{off}) in the control off-resonance experiment where an "empty" proton NMR spectral region was selectively irradiated. Those cyt *c* $^1H-^{15}N$ cross-peaks that show a decrease in intensity in the on-resonance experiment, indicated by an increase in I_{off}/I_{on}, are considered to be at the intermolecular interface. The temperature of the experiments was lowered from 25 to 15 °C to increase the protein rotational correlation time and thus enhance the saturation transfer rate.

In a control on-resonance experiment in which the aliphatic hydrogens on isolated ^2H- and ^{15}N-enriched cyt *c* were saturated, we unexpectedly observed that several NH resonances exhibited a decrease in peak height. Additional controls verified that the effect was not mediated through accidental irradiation of the water resonance. Apparently, the deuteration of the heme and aliphatics was not entirely complete.

Two strategies were employed to minimize the residual intramolecular saturation transfer in cyt *c*. First, three separate experiments were carried out with saturation frequencies of 0.2, 1.2, and 2.2 ppm with a very narrow bandwidth of 1 ppm to the sample of cyt *c* alone. The purpose was to find a condition under which the saturation of heme protons of cyt *c* can be minimized.

The mean values of I_{off}/I_{on} for the amide protons of isolated cyt *c* were found to be 1.25, 1.40, and 1.41 for the saturation frequency centers at 0.2, 1.2, and 2.2 ppm, respectively. It is clear that saturation at 0.2 ppm is the best to carry out the saturation transfer experiment. The second strategy employed was to plot I_{off}/I_{on} for cyt *c* in the presence of cyt b_5 versus I_{off}/I_{on} for cyt *c* alone. Assuming that the residual intramolecular saturation of cyt *c* amide protons will not be affected by complex formation, the plot described above can be used to separate the intermolecular proton saturation transfer from the unwanted intramolecular proton saturation. Figure 6 shows such a plot when the saturation frequency was set to 0.2 ppm. A linear fit of the data was carried out, yielding a line with a slope of 1.4 and a correlation coefficient, *R*, of 0.95. The slope is expected to be larger than unity because (intramolecular) cross saturation in cyt *c* is more efficient in the larger complex (the cross-saturation rate is proportional to the rotational correlation time). Several data points in Figure 6 are seen to deviate more than one standard deviation from the linear fit. These points all have a higher value of I_{off}/I_{on} corresponding to stronger cross saturation in the complex than in cyt *c* alone (note that the reverse is physically improbable). The outliers, corresponding to residues Gln12, Lys13, Gln16, Phe82, and Lys87, are thus likely to be at the interface of cyt *c* with cyt b_5. A similar plot of the independent data using a saturation frequency of 1.2 ppm also shows three outliers (Gln12, Lys13, and Gln16), but not Phe82 and Lys87 (see Figure 6B in the Supporting Information). The data using a saturation frequency of 2.2 ppm shows no outliers, likely due to masking by the overall increase in the level of cross saturation, as discussed above (data not shown).

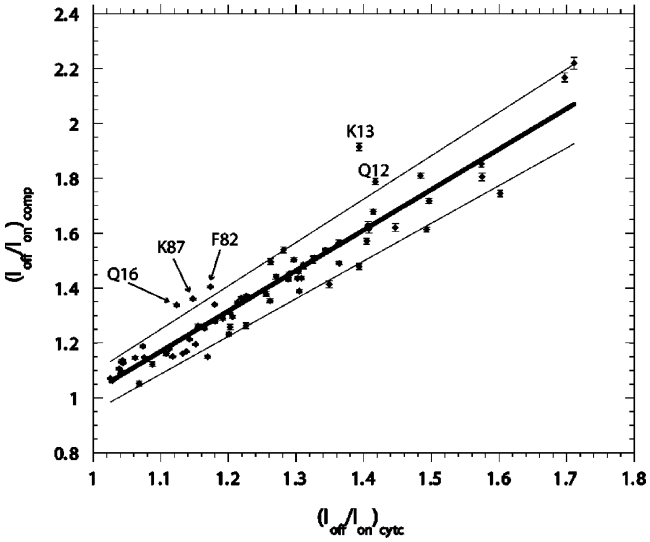

FIGURE 6: Intensity ratio I_{off}/I_{on} of complexed cyt *c* amide proton resonances without (I_{off}) and with (I_{on}) the saturation of aliphatic protons, vs the same ratio for uncomplexed cyt *c*. The saturation center was at 0.2 ppm. The saturation bandwidth was 1 ppm in both cases. The middle line represents the mean chemical shift change, and the top and bottom line signify the mean value ± one standard deviation.

Taken together, the cross-saturation data provides strong evidence that Gln12, Lys13, and Gln16 are at the interface. The evidence for Phe82 and Lys87 is weaker. However, all five residues comprise a subset of residues identified with chemical shift mapping data. As such, the cross-saturation data provide direct support for the idea that the interface is indeed located at the residues inferred from shift mapping.

Calculation of a Cyt c−Cyt b_5 Complex Using NMR Constraints. HADDOCK (High Ambiguity Driven Protein−Protein Docking) enables one to dock two proteins using constraints obtained from biochemical or biophysical interaction data. We used the data obtained from our cross-saturation and chemical shift perturbation NMR experiments on both cyt *c* and cyt b_5 to calculate low-energy complexes of the proteins (*29*). The NMR structure of horse cyt *c* (2GIW) and the crystal structure of bovine cyt b_5 (1CYO) were used as the starting structures. Briefly, in the first stage of the program, the two proteins are docked as rigid bodies, where the docking interface is defined by a combination of experimental NMR restraints and intermolecular energy. In the second stage, the side chains and the backbone at the interface are allowed to move and adopt an optimal conformation. The final stage is refinement of the complex in explicit water, allowing also backbone adaptation. According to the established criteria of HADDOCK, those residues that are solvent exposed and that show chemical shift perturbation, a decrease in peak height during saturation transfer, or a change in dynamics upon binding were considered to be "active" residues for constraining the docking interface. The "passive" residues correspond to the residues that are surface neighbors of the active residues and also have a high solvent accessibility. On the basis of NMR titration and saturation transfer data (this work and ref *29*) and solvent accessibility of residues, 12 amino acids of cyt *c* (Asp2, Lys13, Gln16, Lys72, Gly77, Ile81, Ala83, Ile85, Lys86, Lys87, Lys88, and Thr89) and 10 residues of cyt b_5 (His26, Gly38, Gly41, Gly42, Glu44, Glu59, Asp60, Val61,

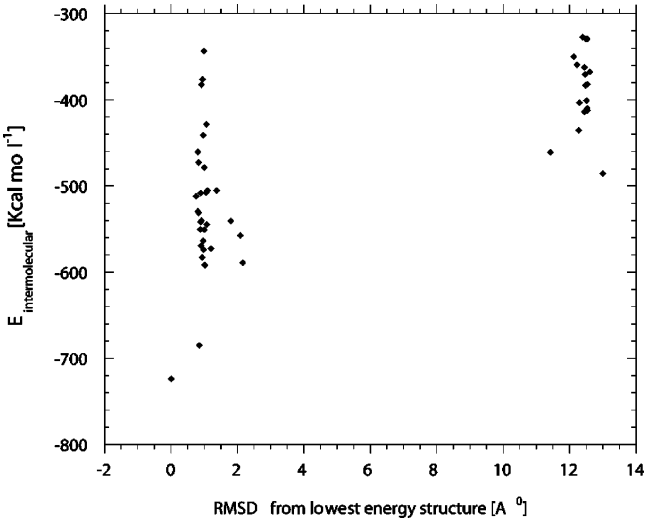

FIGURE 7: Intermolecular energies for the 50 best cyt $c-$cyt b_5 complexes in water vs the rmsd between the interface atoms and those of the lowest-energy complex. The intermolecular energy corresponds to the sum of the ambiguous intermolecular restraints, van der Waals, and electrostatic energy terms. The nonbonded energies were calculated with OPLS parameters using a 8.5 Å cutoff. The complexes were computed with HADDOCK (*30*). The clustering was based on the pairwise backbone rmsd using a 1 Å cutoff.

Gly62, and Ser64) were used as active ambiguous intermolecular restraints. By displaying these amino acids on the surface of the free structures, we defined seven passive amino acids for cyt *c* (His26, Arg38, Pro44, Gly56, Lys60, Glu62, and Lys79) and four passive amino acids for cyt b_5 (Glu37, Pro40, Val45, and Glu48). Considering the proposed importance of the C6-propionate group of heme of cyt b_5 in the formation of the complex (*5*, *54*−*56*), the ambiguous distance restraint file was modified to include the carboxylic oxygens of heme 6-propionate as active atoms excluding other parts of the heme. During the torsion angle space simulated annealing and the refinement in water, the amino acids at the interface are allowed to move to optimize the interface packing. The interfacial residues that are allowed to move consisted of residues in the ambiguous distance restraint file of both molecules.

Figure 7 shows the intermolecular energy as a function of the root-mean-square deviation (rmsd) of the backbone atoms from the lowest-energy structure for the 50 structures. Two clusters could be identified on the basis of pairwise backbone rmsd values using a 1.0 Å cutoff. The first cluster contains the overall lowest-energy structure as well as the largest number of structures. The statistical analysis of the clusters is summarized in Table 1. The average rmsd's from the lowest-energy structure in cluster A are 0.911 and 12.46 Å for models in cluster A and cluster B, respectively, indicating substantially different conformations for the clusters. The difference in the average value of intermolecular energies for clusters A and B, −526 and −386 kcal/mol, respectively, is too small to serve as a selection criterion. For both clusters, the major contribution to $E_{\text{intermolecular}}$ is from $E_{\text{electrostatic}}$, signifying the importance of electrostatic interactions in complex formation. The average values of buried surface areas for the two clusters are 1152 and 1042 Å^2, respectively. Also, these measures were not sufficiently different for discriminating between the clusters.

Information concerning the distance between the heme groups in the cyt $c-$cyt b_5 complex has been sought through fluorescence quenching experiments involving fluorescent derivatives of cyt *c* in which the prosthetic group is modified by the replacement of the central iron atom with zinc or by complete removal of the central metal atom (*1*). The Fe−Fe distance estimated in both these studies for the cyt $c-$cyt b_5 complex was ∼18 Å, while the heme planes are approximately perpendicular. The average Fe−Fe distance in cluster A is 16.75 Å and in cluster B 18.62 Å. Both of these are in good agreement with the fluorescence data. Regretfully, this measure does not discriminate between the two clusters.

Calculation of the Chemical Shifts Expected from the Docked Complex. In an attempt to discriminate between the clusters, we selected the best structure of each cluster and calculated what can be predicted for the amide proton chemical shift changes upon docking in each complex. Using ShiftCalc (*46*−*48*), we obtained a correlation between the sequence location and sign of the predicted amide proton chemical shifts and the experimentally observed chemical shifts for the best structure of cluster A (panels A and B of Figure 8). The correspondence is much weaker for the best structure of cluster B, especially for the region around residue 13 (panel C of Figure 8). Interestingly, the computational analysis shows that the chemical shifts observed in cyt *c* upon complexation with cyt b_5 are almost exclusively caused by the proximity of the edge of the heme of cyt b_5. For cluster A, the ring current-induced magnetic dipole on the cyt b_5 heme adds to the magnetic field sensed by the amide protons of cyt *c* in the areas around residues Ile85 and Lys13 leading to a NMR frequency increase (shifts to a higher number of parts per million as observed). For cluster B, it is predicted that the intermolecular ring current effect would lead to shifts to lower parts per million values for the area around Lys13. Ring current shielding analysis is well-established in NMR spectroscopy, and the direction of the shifts is predicted very reliably. Hence, our calculations suggest that cluster A is the best representation of the complex.

Interestingly, the ShiftCalc calculation also predicts the experimental observation of a much larger chemical shift change for the amide protons of cyt *c* upon complexation with cyt b_5 (this study) as compared to the chemical shift change for the amide protons of cyt b_5 upon complexation with cyt *c* (*29*). This is understandable when considering the fact that ≅11% of the heme in cyt b_5 is solvent accessible and can closely approach its interaction partner while the heme of cyt *c* is almost entirely embedded in the protein matrix (only 3.5% of the cyt *c* heme is solvent accessible) and remains distant from cyt b_5 in the complex.

Comparison with Other Work. The average rmsd positional differences when superimposing all atoms in the best 10 complexes (all fall in cluster A) are 0.90 and 1.01 Å for the interface residues of cyt *c* and cyt b_5, respectively. The slightly higher rmsd for cyt b_5 compared to that for cyt *c* may indicate a more diffuse nature of the interaction surface of cyt b_5. This may be another reason for the smaller magnitude of chemical shift changes observed when isotope-enriched cyt b_5 is titrated with cyt *c* (*29*). Three solutions (all of cluster A), based on the lowest intermolecular energy, were selected to represent the models of the cyt $c-$cyt b_5 complex.

Table 1: Statistical Analysis of the 50 Lowest-Energy Structures

	rmsd (Å)[a]	rmsd minimum (Å)[b]	no. of structures	E_{inter}[c]	E_{clec}	E_{vdw}	E_{AIR}	buried surface area (Å^2)
Cluster A	0.91 ± 0.2	0.91 ± 0.2	27	−526.6 ± 28.6	−501.1 ± 83.2	−34.3 ± 5.3	8.8 ± 1.2	1152.2 ± 59.3
Cluster B	0.72 ± 0.3	12.5 ± 0.1	9	−386.8 ± 28.6	−368.6 ± 27.6	−27.4 ± 4.4	9.2 ± 0.9	1042.1 ± 42.7

[a] Average rmsd and standard deviation from the lowest-energy structure of the cluster. [b] Average rmsd and standard deviation from the lowest-energy structure of all calculated structures. [c] E_{inter} is the intermolecular energy. It is the sum of E_{clec} (electrostatic energy), E_{vdw} (van der Waals energy), and E_{AIR} (energy of the ambiguous intermolecular restraints).

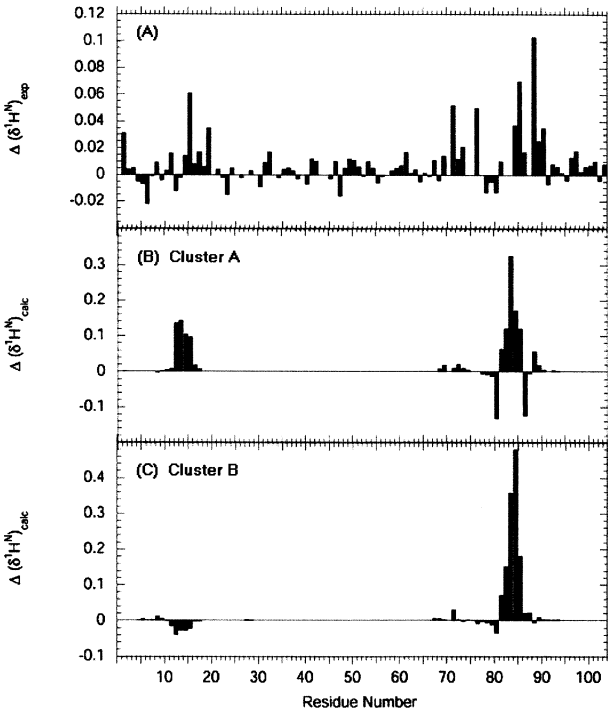

FIGURE 8: Comparison of the (A) experimentally determined chemical shift changes for the amide protons of 0.8 mM cyt *c* upon addition of 1.2 mM cyt b_5 with the calculated amide proton chemical shift change (*46*−*48*) for (B) the lowest-energy structure of cluster A and (C) the lowest-energy structure of cluster B. The clusters are defined in Figure 7.

The molecular interface of the lowest-energy solution of cluster A is shown in Figure 9A. Although the interaction surface of horse cyt *c*, which was used in this study, is similar to the one predicted by Northrup et al. (*13*), using yeast iso-1-cyt *c*, the electrostatic pairing of residues is different. While Northrup and co-workers proposed that the most frequently encountered docking geometries involved hydrogen bonding interactions between Lys13, Lys87, Lys86, and trimethyllysine 72 of yeast cyt *c* and Glu48, Glu56, Asp60, and heme 6-propionate of cyt b_5, respectively, our docking predicts the formation of salt bridges between Lys72 of cyt *c* and Asp60 of cyt b_5, Lys73 of cyt *c* and Glu56 and Asp60 of cyt b_5, Lys86 of cyt *c* and Glu43 and Glu44 of cyt b_5, Lys87 of cyt *c* and Glu48 of cyt b_5, and Lys88 of cyt *c* and Glu44 of cyt b_5 (shown in Figure 10). Other interactions that are present are hydrogen bonds between HG1 of Thr89 (cyt *c*) and OE1 and OE2 of Glu44 (cyt b_5), the ϵ-amino group of Lys13 (cyt *c*) and the carbonyl oxygen of Gly41 (cyt b_5), and the side-chain amide of Gln16 (cyt *c*) and heme 6-propionate (cyt b_5). Important hydrophobic contacts are between residues Lys13, Gln16, Ile81, Phe82, Ala83, Lys86, and Lys87 of cyt *c* and Gly41, heme, Asp60 and Val61, Val61 and heme, Asn57 and Val61, Glu44 and Gly 42, and Glu44 of cyt b_5, respectively. The distance between the two irons is 16.05 Å, whereas the two heme planes are nearly perpendicular.

The interaction surface of solution 2 is somewhat different than that in solution 1. While Lys72 of cyt *c* can make salt bridges with both Glu56 and Asp60 of cyt b_5, the amide group of Ala83 and carbonyl oxygen of Gly84 of cyt *c* are within hydrogen bonding distance of the carbonyl oxygen of Asp60 and the side-chain amide hydrogen of Asn57 of cyt b_5. There are important hydrophobic contacts in the cyt *c*−cyt b_5 interface between residues Lys72 of cyt *c* and Asp60 of cyt b_5, between Ile81 of cyt *c* and Asp60, Val 61, and Gly62 of cyt b_5, between Phe82 of cyt *c* and the heme of cyt b_5, between Ala83 of cyt *c* and Asp60 of cyt b_5, between Lys86 of cyt *c* and Glu44 and Val45 of cyt b_5, between Lys87 of cyt *c* and Glu44 of cyt b_5, and between Lys86 of cyt *c* and Val45 of cyt b_5. The interaction surface of solution 3 is similar to that of solution 2.

The molecular interface of the lowest-energy solution of cluster B is shown in Figure 9B. The molecular interface of the lowest-energy solution of cluster B consists of salt bridges between Lys13 of cyt *c* and Asp60 of cyt b_5, Lys72 of cyt *c* and Glu44 of cyt b_5, Lys79 of cyt *c* and Glu48 of cyt b_5, and Lys86 of cyt *c* and heme 6-propionate of cyt b_5. Other interactions present in solution 1 are hydrogen bonds of Lys87 of cyt *c* with Ser64 and Gly62 of cyt b_5. Important hydrophobic contacts are between residues Ile81 of cyt *c* and Glu44, Glu48, and Val45 of cyt b_5, A81 of cyt *c* and Gly41 and Gly42 of cyt b_5, Ile85 of cyt *c* and Val61 of cyt b_5, G84, K86, and K87 of cyt *c* and heme of cyt b_5.

The molecular interface of the three solutions in cluster A is consistent with the earlier observation of the importance of charged residues 43, 44, 48, 56, and 60 of cyt b_5 and the heme 6-propionate in the complex formation. Replacement of charged residues 43, 44, 48, and 60 of cyt b_5 with their neutral analogues (*8*) and of residues 44, 48, 54, and 60 (as well as multiple replacements) with Ala by site-directed mutagenesis results in an increase in the dissociation constant of the complex (*12*, *57*). However, removal of Glu44, Glu48, and Asp60 and modification of the heme propionate yield an only 14% decrease in the free energy of association with cyt *c* (*9*). This observation may be explained by the fact that Glu44 can transfer its interactive function to its neighbor Glu43, while Asp60 can hand over its interactive function to Glu59 and vice versa as observed in the case of solutions 1, 2, and 3. Dimethyl esterification of the heme propionates of cyt b_5 diminishes the binding and electron transfer rate, indicating the importance of heme propionates in complex formation (*3*). Measurement of the rate of interprotein electron -transfer rates and binding constants with numerous cyt b_5 mutants by McLendon, Huang, and colleagues is consistent with our proposed binding interface (*57*). Their extensive studies led the investigators to conclude that

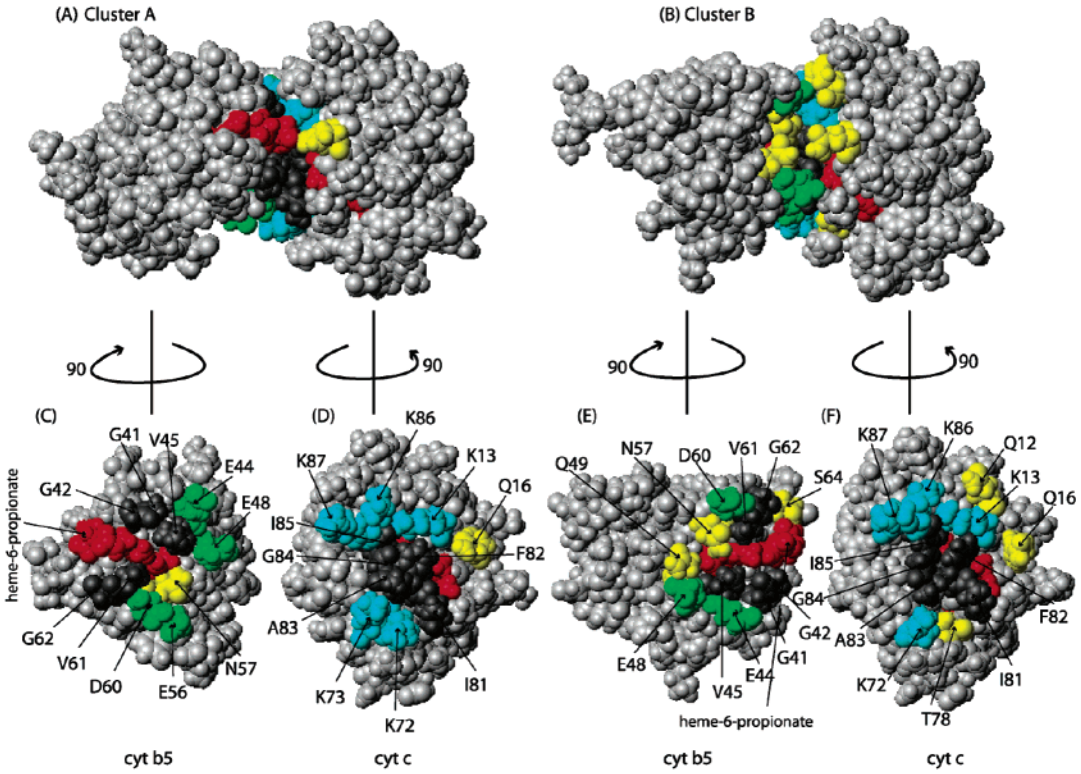

FIGURE 9: Lowest-energy cyt c−cyt b_5 complex of cluster A and cluster B. Positive, negative, polar uncharged, and hydrophobic interfacial residues are colored cyan, green, yellow, and dark gray, respectively. In the bottom panel, cyt c and cyt b_5 are rotated along their y-axes by 90° in opposite directions to display their interface.

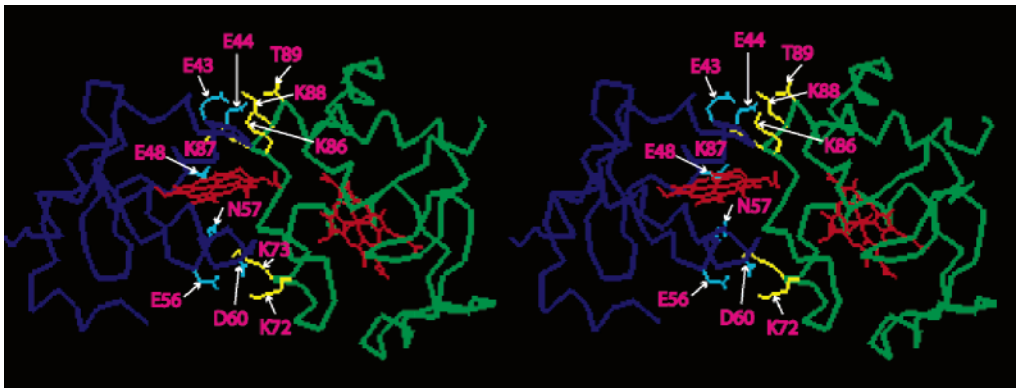

FIGURE 10: Stereoview of the Cα trace of the lowest-energy cyt c−cyt b_5 complex in cluster A. It illustrates the predicted salt bridges between the lysines of cyt c and the acidic glutamates and aspartates of cyt b_5.

electrostatic interactions participate primarily in maintaining the stability of the complex whereas the hydrophobic residues flanking the heme regulate the electron transfer rates.

The molecular interfaces of these structural models are consistent with the importance of cyt c lysine residues, Lys72, Lys73, Lys86, Lys87, and Lys88, in the formation of the complex. These residues also contribute to a large molecular dipole which interacts with an oppositely charged molecular dipole on cyt b_5 to precollisionally orient the two proteins (*1*). Other cyt c residues involved in hydrogen bonds are Lys13 and Thr89. The important hydrophobic residues are Ile81 and Phe82. The findings described above may be relevant for the physiological function of cyt c. For example, in the crystal structure of the cyt c−cyt c peroxidase complex, these same residues have been reported to be involved in interprotein interactions. Indeed, Gln16 of cyt c was seen to be in close contact with Ala193 of cyt c peroxidase, and Lys 87 of cyt c was proposed to be a hydrogen bond donor to Asp34 of the peroxidase.

Very recently, another group has used NMR chemical shift perturbations and docking methods to propose a model for the interaction of bovine ferricyt b_5 with yeast iso-1-ferri and ferrocyt c (*58*). While the equilibrium dissociation constant and general chemical shift perturbation patterns are similar to those in our case, their docking results are compatible with a complex, described by a rather diffuse intermolecular interface. We determined, in contrast, a cluster with essentially one major structure, which may be the average of a dynamic complex. There can be several reasons for this. First, we are working with different species of cyt c. A close look at the cyt b_5 interface of horse and yeast cyt c (Figure 5A,B) reveals some differences. Importantly, residues 86−89 constitute a basic patch on the cyt c surface. Each patch contains three lysines, while the fourth residue

is a glutamic acid in the yeast protein and a threonine in the horse cytochrome. This amino acid substitution will increase the negative charge on the yeast patch and render it less attracted to the anionic surface of cyt b_5. As a consequence, the binding interface may be destabilized and more diffuse in the yeast protein. Important hydrophobic residues such as Ile81, Ala83, and Ile85 in horse cyt *c* are replaced with Ala81, Gly83, and Leu85. Cyt *c* residues 8, 9, 12, 13, and 15 which are part of the binding interface are not conserved between the two sources of cyt *c*. Residues 8, 9, 12, and 15 are involved in the yeast cyt *c*, while only residues 12 and 13 of horse cyt *c* are at the interface. Second, we have incorporated more data (saturation transfer, chemical shift perturbation of methyl group protons, and calculation of the chemical shifts predicted by the model complex with ShiftCal). Thus, it is possible to define the interface on cyt b_5 and cyt *c* more precisely during computing. In turn, this required use of a smaller number of passive residues in the calculation of the docked complex and likely accounts for the major difference between the extent of our interface and that of Ubbink and co-workers. They used a total of 26 active and 43 passive ambiguous intermolecular restraints in their calculations (*58*). In contrast, our HADDOCK calculations employed a total of 23 active but only 11 passive restraints. Passive residues are surface residues which were not identified experimentally, but are included in the calculations because they are in direct contact with the active residues. Fewer passive residues allow a more precise interface determination. In addition, the carboxylate oxygens of the cyt b_5 heme 6-propionate were considered to be active residues in our calculation in contrast to the calculation by Volkov et al., where the 5-CH_3 and 6-α-porphyrin CH_2 groups were deemed active (*58*). Third, our titration of reduced horse cyt *c* with high concentrations of reduced bovine cyt b_5 did not reveal any evidence of a 1:2 complex as reported by Volkov et al., for their system. Therefore, there was no need to invoke a ternary complex with higher stoichiometry in our system.

SUMMARY

In this work, chemical shift mapping and cross-saturation experiments were used to identify the residues of horse cyt *c* involved in the binding interface with bovine cyt b_5. Our results show that the association between ferrous cyt *c* and ferrous cyt b_5 occurs in a 1:1 stoichiometry. This is in contrast to a previous study of a complex between reduced yeast iso-1- cyt *c* and reduced rabbit cyt b_5 (*52*) which report the formation of a 2:1 adduct at high concentrations of cyt *c*.

Mapping chemical shift variations and intensity changes upon cross-saturation transfer on the solution structure of cyt *c* reveals a single interaction patch on cyt *c*. This patch is not consistent with the earlier Salemme model which involves tuna cyt *c* residues Lys27 and Lys79. These residues are far from the interfacial region as derived from the experimental NMR data. Our NMR data reveal the involvement of Lys13, Lys72, Lys86, Lys87, and Lys88, corroborating the model proposed by Northrup with yeast cyt *c* (*13*). NMR data from the current experiments, as well as NMR data delineating the interaction interface of cyt b_5, were used in the protein docking program HADDOCK to calculate a structural model for the complex. From the protein docking program, we obtained two different clusters of possible complex structures. One of these clusters could be ruled out on the basis of ring current calculations. The three best structural models in the remaining cluster represent the cyt *c*−cyt b_5 complex in solution. The average buried surface area is 1152 ± 50 Å. The iron−iron distance is 16 Å, in contrast to the distance of 20 Å obtained in a docking model for yeast iso-1-cyt *c* and rabbit cyt b_5 (*13*).

Although the interaction surface of cyt *c* in our experimentally constrained model of the cyt *c*−cyt b_5 complex is similar to the one predicted by Northrup (*13*), the electrostatic pairing of residues is different, suggesting that similar but nonidentical complexes are formed by homologous proteins from different species.

SUPPORTING INFORMATION AVAILABLE

NMR spectra of the methyl group region of $^1H-^{13}C$ HSQC spectra of free and bound cyt *c* and the intensity ratio (I_{off}/I_{on}) of complexed cyt *c* amide resonances at 1.2 ppm. This material is available free of charge via the Internet at http://pubs.acs.org. The pdf file of Figure 10 is available upon request.

REFERENCES

1. Mauk, A. G., Mauk, M. R., Moore, G. R., and Northrup, S. H. (1995) Experimental and theoretical analysis of the interaction between cytochrome *c* and cytochrome b_5, *J. Bioenerg. Biomembr. 27*, 311−30.
2. Mauk, M. R., and Mauk, A. G. (1982) Interaction between cytochrome b_5 and human methemoglobin, *Biochemistry 21*, 4730−4.
3. Mauk, M. R., Mauk, A. G., Weber, P. C., and Matthew, J. B. (1986) Electrostatic analysis of the interaction of cytochrome *c* with native and dimethyl ester heme substituted cytochrome b_5, *Biochemistry 25*, 7085−91.
4. Mauk, M. R., Barker, P. D., and Mauk, A. G. (1991) Proton linkage of complex formation between cytochrome *c* and cytochrome b_5: Electrostatic consequences of protein−protein interactions, *Biochemistry 30*, 9873−81.
5. Salemme, F. R. (1976) An hypothetical structure for an intermolecular electron transfer complex of cytochromes *c* and b_5, *J. Mol. Biol. 102*, 563−8.
6. Wendoloski, J. J., Matthew, J. B., Weber, P. C., and Salemme, F. R. (1987) Molecular dynamics of a cytochrome *c*-cytochrome b_5 electron transfer complex, *Science 238*, 794−7.
7. Durham, B., Fairris, J. L., McLean, M., Millett, F., Scott, J. R., Sligar, S. G., and Willie, A. (1995) Electron transfer from cytochrome b_5 to cytochrome *c*, *J. Bioenerg. Biomembr. 27*, 331−40.
8. Rodgers, K. K., Pochapsky, T. C., and Sligar, S. G. (1988) Probing the mechanisms of macromolecular recognition: The cytochrome b_5-cytochrome *c* complex, *Science 240*, 1657−9.
9. Rodgers, K. K., and Sligar, S. G. (1991) Mapping electrostatic interactions in macromolecular associations, *J. Mol. Biol. 221*, 1453−60.
10. Stayton, P. S., Fisher, M. T., and Sligar, S. G. (1988) Determination of cytochrome b_5 association reactions. Characterization of metmyoglobin and cytochrome P-450cam binding to genetically engineered cytochrome b_5, *J. Biol. Chem. 263*, 13544−8.
11. Bagby, S., Barker, P. D., Guo, L. H., and Hill, H. A. (1990) Direct electrochemistry of protein−protein complexes involving cytochrome *c*, cytochrome b_5, and plastocyanin, *Biochemistry 29*, 3213−9.
12. Sun, Y. L., Wang, Y. H., Yan, M. M., Sun, B. Y., Xie, Y., Huang, Z. X., Jiang, S. K., and Wu, H. M. (1999) Structure, interaction and electron transfer between cytochrome b_5, its E44A and/or E56A mutants and cytochrome *c*, *J. Mol. Biol. 285*, 347−59.

13. Northrup, S. H., Thomasson, K. A., Miller, C. M., Barker, P. D., Eltis, L. D., Guillemette, J. G., Inglis, S. C., and Mauk, A. G. (1993) Effects of charged amino acid mutations on the bimolecular kinetics of reduction of yeast iso-1-ferricytochrome *c* by bovine ferrocytochrome b_5, *Biochemistry 32*, 6613−23.
14. Willie, A., McLean, M., Liu, R. Q., Hilgen-Willis, S., Saunders, A. J., Pielak, G. J., Sligar, S. G., Durham, B., and Millett, F. (1993) Intracomplex electron transfer between ruthenium-65-cytochrome b_5 and position-82 variants of yeast iso-1-cytochrome *c*, *Biochemistry 32*, 7519−25.
15. McLendon, G. L., Winkler, J. R., Nocera, D. G., Mauk, M. R., Mauk, A. G., and Gray, H. B. (1985) Quenching of zinc-substituted cytochrome-*c* excited-states by cytochrome-b_5, *J. Am. Chem. Soc. 107*, 739−40.
16. Kornblatt, J. A., Hoa, G. H. B., Eltis, L., and Mauk, A. G. (1988) The effects of pressure on porphyrin-*c*-cytochrome-b_5 complex-formation, *J. Am. Chem. Soc. 110*, 5909−11.
17. Kornblatt, J. A., Kornblatt, M. J., Hoa, G. H., and Mauk, A. G. (1993) Responses of two protein−protein complexes to solvent stress: Does water play a role at the interface? *Biophys. J. 65*, 1059−65.
18. Burch, A. M., Rigby, S. E., Funk, W. D., MacGillivray, R. T., Mauk, M. R., Mauk, A. G., and Moore, G. R. (1990) NMR characterization of surface interactions in the cytochrome b_5-cytochrome *c* complex, *Science 247*, 831−3.
19. Guillemette, J. G., Barker, P. D., Eltis, L. D., Lo, T. P., Smith, M., Brayer, G. D., and Mauk, A. G. (1994) Analysis of the bimolecular reduction of ferricytochrome *c* by ferrocytochrome b_5 through mutagenesis and molecular modelling, *Biochimie 76*, 592−604.
20. Hom, K., Ma, Q. F., Wolfe, G., Zhang, H., Storch, E. M., Daggett, V., Basus, V. J., and Waskell, L. (2000) NMR studies of the association of cytochrome b_5 with cytochrome *c*, *Biochemistry 39*, 14025−39.
21. Ubbink, M., Ejdeback, M., Karlsson, B. G., and Bendall, D. S. (1998) The structure of the complex of plastocyanin and cytochrome f, determined by paramagnetic NMR and restrained rigid-body molecular dynamics, *Structure 6*, 323−35.
22. Veitch, N. C., Whitford, D., and Williams, R. J. (1990) An analysis of pseudocontact shifts and their relationship to structural features of the redox states of cytochrome b_5, *FEBS Lett. 269*, 297−304.
23. Worrall, J. A., Liu, Y., Crowley, P. B., Nocek, J. M., Hoffman, B. M., and Ubbink, M. (2002) Myoglobin and cytochrome b_5: A nuclear magnetic resonance study of a highly dynamic protein complex, *Biochemistry 41*, 11721−30.
24. Moore, G. R., Cox, M. C., Crowe, D., Osborne, M. J., Rosell, F. I., Bujons, J., Barker, P. D., Mauk, M. R., and Mauk, A. G. (1998) Nϵ,Nϵ-dimethyl-lysine cytochrome *c* as an NMR probe for lysine involvement in protein−protein complex formation, *Biochem. J. 332* (Part 2), 439−49.
25. Eley, C. G., and Moore, G. R. (1983) ^{1}H-NMR investigation of the interaction between cytochrome *c* and cytochrome b_5, *Biochem. J. 215*, 11−21.
26. Whitford, D., Concar, D. W., Veitch, N. C., and Williams, R. J. (1990) The formation of protein complexes between ferricytochrome b_5 and ferricytochrome *c* studied using high-resolution ^{1}H NMR spectroscopy, *Eur. J. Biochem. 192*, 715−21.
27. Whitford, D., Gao, Y., Pielak, G. J., Williams, R. J., McLendon, G. L., and Sherman, F. (1991) The role of the internal hydrogen bond network in first-order protein electron transfer between *Saccharomyces cerevisiae* iso-1-cytochrome *c* and bovine microsomal cytochrome b_5, *Eur. J. Biochem. 200*, 359−67.
28. Guiles, R. D., Sarma, S., DiGate, R. J., Banville, D., Basus, V. J., Kuntz, I. D., and Waskell, L. (1996) Pseudocontact shifts used in the restraint of the solution structures of electron transfer complexes, *Nat. Struct. Biol. 3*, 333−9.
29. Shao, W., Im, S. C., Zuiderweg, E. R., and Waskell, L. (2003) Mapping the binding interface of the cytochrome b_5-cytochrome *c* complex by nuclear magnetic resonance, *Biochemistry 42*, 14774−84.
30. Dominguez, C., Boelens, R., and Bonvin, A. M. (2003) HADDOCK: A protein−protein docking approach based on biochemical or biophysical information, *J. Am. Chem. Soc. 125*, 1731−7.
31. Morelli, X., Dolla, A., Czjzek, M., Palma, P. N., Blasco, F., Krippahl, L., Moura, J. J., and Guerlesquin, F. (2000) Heteronuclear NMR and soft docking: An experimental approach for a structural model of the cytochrome *c*553-ferredoxin complex, *Biochemistry 39*, 2530−7.
32. Morelli, X., Czjzek, M., Hatchikian, C. E., Bornet, O., Fontecilla-Camps, J. C., Palma, N. P., Moura, J. J., and Guerlesquin, F. (2000) Structural model of the Fe-hydrogenase/cytochrome *c*553 complex combining transverse relaxation-optimized spectroscopy experiments and soft docking calculations, *J. Biol. Chem. 275*, 23204−10.
33. Crowley, P. B., Rabe, K. S., Worrall, J. A., Canters, G. W., and Ubbink, M. (2002) The ternary complex of cytochrome f and cytochrome *c*: Identification of a second binding site and competition for plastocyanin binding, *ChemBioChem 3*, 526−33.
34. Ausubel, F. M., Brent, R., and Kingston, R. E. (1997) *Current Protocols in Molecular Biology*, John Wiley & Sons, New York.
35. Miroux, B., and Walker, J. E. (1996) Over-production of proteins in *Escherichia coli*: Mutant hosts that allow synthesis of some membrane proteins and globular proteins at high levels, *J. Mol. Biol. 260*, 289−98.
36. Bridges, A., Gruenke, L., Chang, Y. T., Vakser, I. A., Loew, G., and Waskell, L. (1998) Identification of the binding site on cytochrome P450 2B4 for cytochrome b_5 and cytochrome P450 reductase, *J. Biol. Chem. 273*, 17036−49.
37. Patel, C. N., Lind, M. C., and Pielak, G. J. (2001) Characterization of horse cytochrome *c* expressed in *Escherichia coli*, *Protein Expression Purif. 22*, 220−4.
38. Arslan, E., Schulz, H., Zufferey, R., Kunzler, P., and Thony-Meyer, L. (1998) Overproduction of the *Bradyrhizobium japonicum* c-type cytochrome subunits of the cbb3 oxidase in *Escherichia coli*, *Biochem. Biophys. Res. Commun. 251*, 744−7.
39. Margoliash, E., Frohwirt, N., and Wiener, E. (1959) A study of the cytochrome *c* haemochromogen, *Biochem. J. 71*, 559−70.
40. Delaglio, F., Grzesiek, S., Vuister, G. W., Zhu, G., Pfeifer, J., and Bax, A. (1995) NMRPipe: A multidimensional spectral processing system based on UNIX pipes, *J. Biomol. NMR 6*, 277−93.
41. Koradi, R., Billeter, M., and Wüthrich, K. (1996) MOLMOL: A program for display and analysis of macromolecular structures, *J. Mol. Graphics 14*, 51−5.
42. Takahashi, H., Nakanishi, T., Kami, K., Arata, Y., and Shimada, I. (2000) A novel NMR method for determining the interfaces of large protein−protein complexes, *Nat. Struct. Biol. 7*, 220−3.
43. Kleywegt, G. J. (1995) Dictionaries for Heteros, *CCP4/ESF-EACBM Newsletter on Protein Crystallography*, Vol. 31, pp 45−50, Daresbury Laboratory, Warrington, U.K.
44. Kleywegt, G. J., Zou, J. Y., Kjeldgaard, M., and Jones, T. A. (2001) in *International Tables for Crystallography* (Rossmann, M. G., and Arnold, E., Eds.) pp 353−6, Kluwer Academic Publishers, Dordrecht, The Netherlands.
45. Kleywegt, G. J., Henrick, K., Dodson, E. J., and van Aalten, D. M. (2003) Pound-wise but penny-foolish: How well do micromolecules fare in macromolecular refinement? *Structure 11*, 1051−9.
46. Asakura, T., Taoka, K., Demura, M., and Williamson, M. P. (1995) The Relationship between Amide Proton Chemical-Shifts and Secondary Structure in Proteins, *J. Biomol. NMR 6*, 227−36.
47. Asakura, T., and Williamson, M. P. (1993) Empirical comparisons of models for chemical-shift calculation in proteins, *J. Magn. Reson., Ser. B 101*, 63−71.
48. Williamson, M. P., Asakura, T., Nakamura, E., and Demura, M. (1992) A method for the calculation of protein α-CH chemical shifts, *J. Biomol. NMR 2*, 83−98.
49. Liu, W., Rumbley, J., Englander, S. W., and Wand, A. J. (2003) Backbone and side-chain heteronuclear resonance assignments and hyperfine NMR shifts in horse cytochrome *c*, *Protein Sci. 12*, 2104−8.
50. Feher, V. A., and Cavanagh, J. (1999) Millisecond-timescale motions contribute to the function of the bacterial response regulator protein Spo0F, *Nature 400*, 289−93.
51. Banci, L., Bertini, I., Huber, J. G., Spyroulias, G. A., and Turano, P. (1999) Solution structure of reduced horse heart cytochrome *c*, *J. Biol. Inorg. Chem. 4*, 21−31.
52. Banci, L., Bertini, I., Felli, I. C., Krippahl, L., Kubicek, K., Moura, J. J., and Rosato, A. (2003) A further investigation of the cytochrome b_5-cytochrome *c* complex, *J. Biol. Inorg. Chem. 8*, 777−86.
53. Nakanishi, T., Miyazawa, M., Sakakura, M., Terasawa, H., Takahashi, H., and Shimada, I. (2002) Determination of the interface of a large protein complex by transferred cross-saturation measurements, *J. Mol. Biol. 318*, 245−9.

54. Mathews, F. S., Czerwinski, E. W., and Argos, P. (1979), The Porphyrins (Dolphin, D., Ed.) pp 107−147, Academic Press, Inc., London.
55. Poulos, T. L., and Mauk, A. G. (1983) Models for the complexes formed between cytochrome b_5 and the subunits of methemoglobin, *J. Biol. Chem. 258*, 7369−73.
56. Rodriguez-Maranon, M. J., Qiu, F., Stark, R. E., White, S. P., Zhang, X., Foundling, S. I., Rodriguez, V., Schilling, C. L., III, Bunce, R. A., and Rivera, M. (1996) ^{13}C NMR spectroscopic and X-ray crystallographic study of the role played by mitochondrial cytochrome b_5 heme propionates in the electrostatic binding to cytochrome *c*, *Biochemistry 35*, 16378−90.
57. Ren, Y., Wang, W.-H., Wang, Y.-H., Case, M., Qian, W., McLendon, G., and Huang, Z.-X. (2004) Mapping the electron transfer interface between cytochrome b_5 and cytochrome *c*, *Biochemistry 43*, 3527−36.
58. Volkov, A. N., Ferrari, D., Worrall, J. A. R., Bonvin, A. M. J. J., and Ubbink, M. (2005) The orientations of cytochrome *c* in the highly dynamic complex with cytochrome b_5 visualized by NMR and docking using HADDOCK, *Protein Sci. 14*, 799−811.
59. Goddart, T. D., and Kneller, D. G. (2002) *SPARKY 3*, University of California, San Francisco.

BI050482X